Microfluidics and Nanofluidics (2020) 24:54
https://doi.org/10.1007/s10404-020-02357-z

RESEARCH PAPER

Thermally driven pumps and diodes in multistage assemblies consisting of microchannels with converging, diverging and uniform rectangular cross sections

Guillermo López Quesada[1,2] · Giorgos Tatsios[1] · Dimitris Valougeorgis[1] · Marcos Rojas-Cárdenas[2] · Lucien Baldas[2] · Christine Barrot[2] · Stéphane Colin[2]

Received: 17 February 2020 / Accepted: 2 June 2020

Abstract
Thermal transpiration pumping in multistage assemblies is computationally investigated. Each stage is formed by combining in series-long microchannels with (a) uniform–uniform ("uni–uni"), (b) converging–uniform ("con–uni"), (c) diverging–uniform ("div–uni") and (d) converging–diverging ("con–div") rectangular cross sections. In all four investigated assemblies the generated pressure difference with the associated mass flow rate is fully assessed, in terms of inlet pressure, inclination parameter and number of stages. The analysis is based on linear kinetic modeling and is valid in the whole range of gas rarefaction. It is concluded that the "con–uni" and "div–uni" assemblies provide higher pressure differences and lower mass flow rates than the "uni–uni" assembly and they may be more suitable for specific pumping applications. The characteristics of the "con–uni" and "div–uni" assemblies are very close to each other. The multistage "uni–uni", "con–uni" and "div–uni" assemblies are more stable when operating at small inlet pressures, where the pressure difference remains almost constant in wide ranges of mass flow rate. It is advisable to add as many stages as possible to increase, depending on the application, either the pressure difference or mass flow rate or both. Furthermore, the "con–div" assembly provides smaller pressure differences and mass flow rates than the other three, but it is suitable for diode applications. It is characterized by the so-called blocking inlet pressure, where the deduced pressure difference in the converging and diverging channels is the same. A detailed parametrization of the blocking inlet pressure in terms of inclination ratio, mean height, temperature difference and gas species, has been performed. It is concluded that multistage "con–div" assemblies may be ideally applied as thermally driven microfluidic diodes to control or block the flow, as well as to separate the species in multicomponent gas mixtures.

1 Introduction

Following the pioneering studies of (Maxwell 1878), (Reynolds 1879) and (Knudsen 1909,1910), thermally driven rarefied gas flows in capillaries have been extensively investigated both computationally (Sone 1966; Chernyak et al. 1979; Ohwada et al. 1989; Sharipov and Seleznev 1998;

Electronic supplementary material The online version of this article (https://doi.org/10.1007/s10404-020-02357-z) contains supplementary material, which is available to authorized users.

✉ Dimitris Valougeorgis
diva@mie.uth.gr

Guillermo López Quesada
guillermo.lopez.quesada@gmail.com

Giorgos Tatsios
tatsios@mie.uth.gr

Marcos Rojas-Cárdenas
marcos.rojas@insa-toulouse.fr

Lucien Baldas
lucien.baldas@insa-toulouse.fr

Christine Barrot
christine.barrot@insa-toulouse.fr

Stéphane Colin
stephane.colin@insa-toulouse.fr

[1] Department of Mechanical Engineering, University of Thessaly, 38334 Volos, Greece

[2] Institut Clément Ader (ICA), Université de Toulouse, CNRS, INSA, ISAE-SUPAERO, Mines Albi, UPS, Toulouse, France

Published online: 19 June 2020

Sharipov 1996,1999; Naris et al. 2005; Alexeenko et al. 2006; Graur and Sharipov 2009; Ritos et al. 2011; Pantazis et al. 2013) and experimentally (Rojas-Cárdenas et al. 2013; Yamaguchi et al. 2014; Rojas-Cárdenas et al. 2011). The theoretical justification of such flows, where the gas is flowing from the cold towards the hot regions of the capillary, well-known as thermal creep or thermal transpiration flows, has been provided by (Sone 2000, 2007).

Various geometrical configurations of pumping devices, based on thermal transpiration, known as Knudsen pumps, have been proposed. They are capable of producing a pressure difference, a mass flow rate or both at the same time, without the need of imposing external pressure gradients or using moving mechanical parts. In addition to the typical setup, consisting of narrow and wide channels of constant cross section (Sone et al. 1996; Aoki et al. 2007; Sheng et al. 2014; López Quesada et al. 2019), alternative pump designs have been examined. They include curved channels with constant and varying width (Aoki et al. 2007, 2008; Leontidis et al. 2014; Bond et al. 2014), channels with ratchet-type walls (Chen et al. 2016; Rovenskaya 2020), piping elements arrayed in a matrix form (Bond et al. 2016) and tapered channels (Tatsios et al. 2017).

The range of technological applications is broadened by enhancing pumping effects, based on cascade systems with successive stages and periodic temperature difference at each stage. Each pump stage contains two sub-stages: the pumping sub-stage, which consists of one or more narrow channels or a porous medium or membrane, where a positive temperature gradient is imposed; and the counter-flow sub-stage, which consists of one wide channel, where a negative temperature gradient is imposed. Therefore, thermal transpiration is higher in the pumping sub-stage than in the counter-flow one and net pumping effects are achieved while keeping moderate temperature differences between the reservoirs. The performance characteristics are defined by the achieved mass flow rate and the pressure difference between the inlet and outlet of the pump. The pressure difference is increased with the number of stages.

The range of tentative technological applications of Knudsen pumps in the MEMS industry is broad. Indicatively, Knudsen micropumps may be included in lab-on-chip miniaturized systems for gas sensing and analyzing (Qin and Gianchandani 2014, 2016; Cheng et al. 2017), gas separation (Nakaye et al. 2015; Nakaye and Sugimoto 2016), self-sustained power generation (Zeng et al. 2013), actuation of heat pumps (Kugimoto et al. 2016, 2018) and vacuum pumping (Gupta et al. 2012; An et al. 2014; Toan et al. 2018). However, depending on the target application, the required pump performance can vary considerably. For example, in gas chromatography microanalyzers the mass flow rate should be in the range of $10^{-7} - 10^{-8}$ kg/s, with a pressure difference between $1 - 10$ kPa (Qin and Gianchandani 2014; Kim et al. 2011), while in vacuum maintaining apparatus the sustainable pressure difference should cover several orders of magnitude (from 100 kPa down to 100 Pa) with mass flow rates lower than 10^{-10} kg/s (An et al. 2014; Liu et al. 2009; Beek and Puers 2012).

The first microfabricated single-stage Knudsen pumps are reported in (Vargo 2001), where nanoporous aerogel is used as the transpiration membrane and in (McNamara and Gianchandani 2005), where the pump is formed from microchannel layers of the constant cross section. The fully integrated MEMS-based architecture, introduced in (McNamara and Gianchandani (2005)), has been expanded through a series of works and several multistage Knudsen pumps with various operation characteristics have been developed (Gupta et al. 2012; An et al. 2014; Gupta and Gianchandani 2011; Qin et al. 2015). Recently, an electronic micro gas chromatograph integrating all necessary fluidic components, including a bi-directional Knudsen pump, has been achieved. This Knudsen pump consists of a mesoporous mixed cellulose−ester membrane sandwiched between two glass dies and this architecture significantly reduces fabrication complexity and cost (Qin and Gianchandani 2016; Cheng et al. 2017). So far, however, the pumping effect in all fabricated micropumps is based on thermal transpiration flow through either microchannels of constant cross section or porous media with rather simple geometrical configuration.

Taking into consideration the great potential of these pumps in microfluidics, along with recent advancements in microfabrication, it would be interesting to consider more advanced thermal transpiration pump modules, based on the alternative pump designs described in (Aoki et al. 2007, 2008; Leontidis et al. 2014; Bond et al. 2014,2016; Chen et al. 2016; Tatsios et al. 2017). In particular, the preliminary computational investigation performed in (Tatsios et al. 2017) for temperature-driven flow between converging and diverging plates, paying specific attention to the diode effect (Tatsios et al. 2017; Szalmás et al. 2015; Graur et al. 2016), has indicated that, depending on the operating pressure, additional effects such as bidirectional flow and flow blocking may be observed. In addition, with this design some microfabrication and temperature control pitfalls related to the combination of narrow/wide constant cross-section channels are circumvented. Since nowadays straight and tapered microchannels are manufactured with the same degree of difficulty, assemblies based on the latter design are becoming attractive.

Based on the above, in the present work, the computational methodology introduced in (Tatsios et al. 2017) is extended to computationally investigate and parametrize thermal transpiration pumping in multistage assemblies consisting of series of long rectangular microchannels with converging, diverging and constant cross sections. Combinations of these different channels, taking into account actual manufacturing and operational constraints, are assessed and fully characterized. The characteristic curves of these pumping devices in terms of geometry, operating pressure and number of stages are obtained and their efficiency with regard to the generated mass flow rate and the pressure difference is defined. In addition, thermally driven tapered diodes are investigated, demonstrating their potential as gas controllers and gas mixture separators in microfluidic devices. The most effective of the multistage cascade systems modeled in the present work will be fabricated in a later stage.

2 Pump geometry, flow configuration and characterization parameters

The key elements of all multistage pump designs considered here are long rectangular channels with linearly converging and diverging, as well as constant (uniform) cross sections. To facilitate the presentation and discussion, the corresponding abbreviated names of these channels are "con", "div" and "uni". By combining two rectangular channels of (a) uniform–uniform, (b) converging–uniform, (c) diverging–uniform and (d) converging–diverging cross sections the single stages of four different pump designs, with abbreviated names "uni–uni", "con–uni", "div–uni" and "con–div" respectively, are formed. Finally, by adding in series a number of single stages of the same type the corresponding four proposed multistage assemblies are developed.

The geometry of the single stage of the four investigated assemblies is shown in Fig. 1. In all cases, the single stages consist of two long rectangular channels with constant length L and width (or depth) W between the parallel walls of the channels. Thus, the length of the single stages is always $2L$ and their width is W. The longitudinal direction is denoted by $z \in [0, 2L]$. In the "con–uni", "div–uni" and "con–div" assemblies the variable height $H(z)$ of the tapered channels varies linearly between H_{min} and H_{max}, denoting the smallest and largest distances between the tapered walls, respectively. The tapered channel inclination parameter is always defined as the ratio $\alpha = H_{\text{max}}/H_{\text{min}}$, facilitating the direct comparison between pump setups consisting of

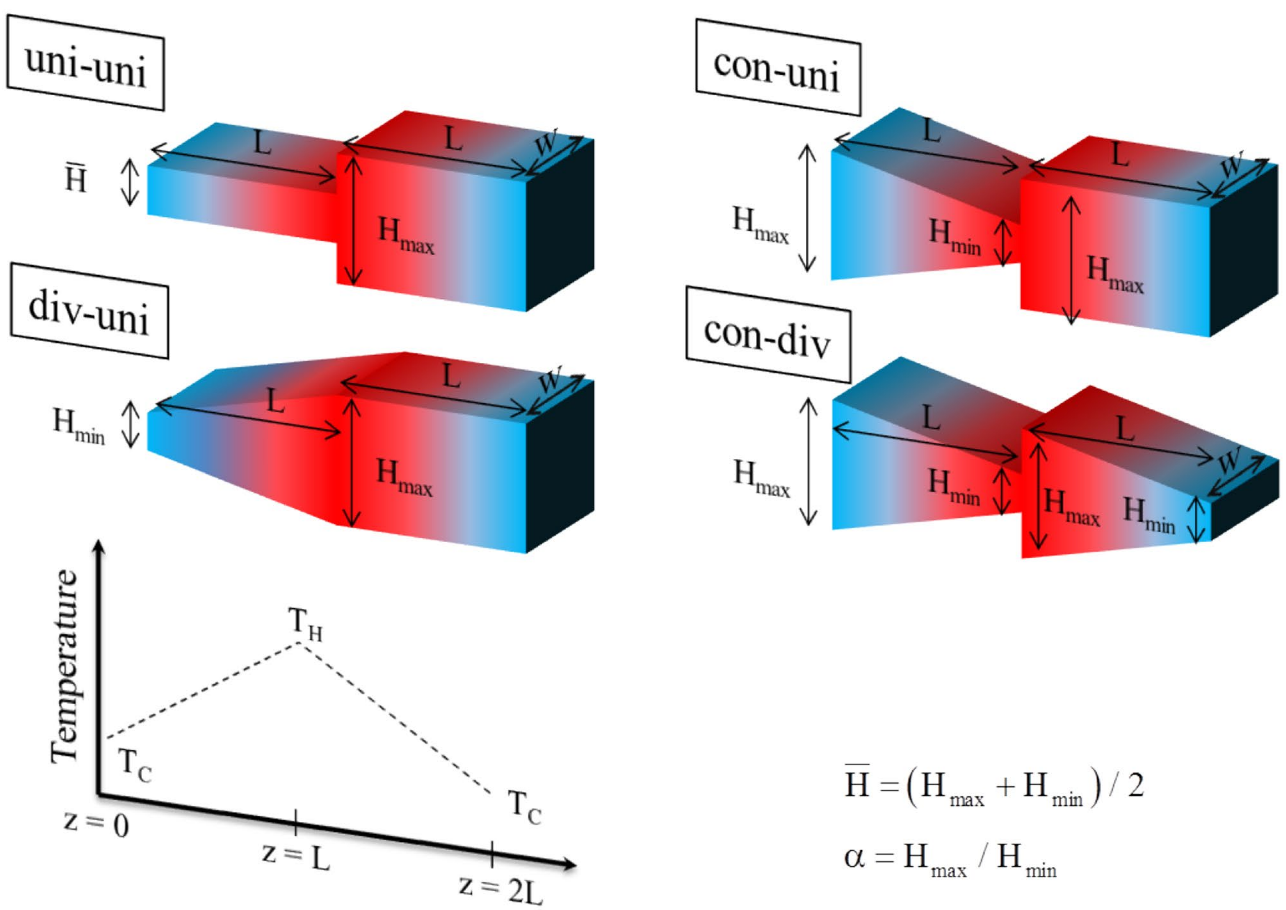

Fig. 1 Schematic view of a single stage of the four assemblies, with uniform–uniform (uni–uni), converging–uniform (con–uni), diverging–uniform (div–uni) and converging–diverging (con–div) rectangular cross sections; the temperature variation along the single-stage assemblies is also shown

converging and diverging channels with the same inclination parameter ($\alpha = \alpha_{\mathrm{con}} = \alpha_{\mathrm{div}}$). The case of $\alpha = 1$ corresponds to the constant cross-section channel. The mean height $\overline{H} = \left(H_{\min} + H_{\max}\right)/2$ is taken as the reference length. In the "con–uni" and "div–uni" assemblies the constant height of the uniform channels is $H_{\max}$ and finally, in the "uni–uni" assembly the two constant heights are $\overline{H}$ and $H_{\max}$. Furthermore, it is assumed that the temperature variation along the single stages is maintained as shown in Fig. 1. The lowest temperature T_C is at $z = 0$ and $z = 2L$, while the highest one T_H is at $z = L$ and along the channel walls the temperature varies linearly between these two limiting values.

As it is well-known, due to the externally imposed and maintained temperature gradients, thermal creep flow is generated from the cold regions at $z = 0$ and $z = 2L$ towards the hot region at $z = L$ and then, due to the increased pressure at the hot region, pressure-driven counter flow is generated from the hot towards the cold regions. By taking $\overline{H} << L$ the flow is considered as fully developed and the end effects are ignored, while the pressure (and density) remains constant in each cross section and varies only in the flow direction, i.e. $P = P(z)$, $z \in [0, 2L]$. In the "uni–uni", "con–uni" and "div–uni" assemblies the pumping sub-stage is clearly the one with the positive temperature gradient, while in the "con–div" assembly, either sub-stage may be the pumping one.

The description provided for the single stages is generalized for the corresponding multistage assemblies. The total length of the assemblies is $N \times (2L)$, where N is the number of stages. The temperature variation is periodic with a period equal to $2L$. The lowest T_C and highest T_H temperature points are located at $z = (2i) \times L$, with $i = 0, 1, ..., N$ and $z = (2i - 1) \times L$, with $i = 1, ..., N$, respectively. The "uni–uni" configuration represents the classical Knudsen pump assembly, while the other three configurations are new proposed designs.

The flow in the above described single and multistage assemblies may be investigated in terms of given geometrical and operational parameters, by extending, in a straightforward manner, the well-known methodology for fully developed flows in single channels of various cross sections (Sharipov and Seleznev 1998; Tatsios et al. 2017; Graur and Ho 2014; Sharipov and Bertoldo 2005; Naris et al. 2014). More specifically, both pressure distribution $P(z)$ and mass flow rate $\dot{m}$ may be obtained by solving the first-order ordinary differential equation (Sharipov 1999; Graur and Ho 2014):

$$\frac{dP}{dz} = -\frac{\upsilon(z)}{WH^2(z)G_P(\delta(z), H/W)}\dot{m} + \frac{G_T(\delta(z), H/W)}{G_P(\delta(z), H/W)}\frac{P(z)}{T(z)}\frac{dT}{dz}, \; z \in [0, N \times (2L)] \tag{1}$$

In Eq. (1), the geometrical parameters of the assembly (L, W, $H(z)$ and N), the temperature variation $T(z)$ and its gradient dT/dz are known. Also, $\upsilon(z) = \sqrt{2R_g T(z)}$ is the most probable molecular speed and R_g is the specific gas constant. In addition, the kinetic coefficients G_P and G_T are obtained by solving the classical fully developed rarefied gas flow through a rectangular channel for the local gas rarefaction parameter

$$\delta(z) = \frac{P(z)H(z)}{\mu(z)\upsilon(z)} \tag{2}$$

and the local cross-section aspect ratio $H(z)/W$. In Eq. (2), $\mu(z)$ is the local dynamic viscosity varying with temperature according to an inverse power-law model, which is consistent with the variable hard sphere molecule hypothesis (Colin 2014). To facilitate the numerical solution of Eq. (1), coefficients G_P and G_T are retrieved from a kinetic database, which has been developed, based on the linearized Shakhov model subject to purely diffuse boundary conditions, in the whole range of $\delta \in [0, \infty)$ and $H(z)/W \in [0, 1]$. Although tabulated values of the coefficients G_P and G_T may be found in (Sharipov 1999; Graur and Ho 2014), they have been recalculated here for the purposes of the present work for much more values of H/W creating a dense database. The kinetic coefficients for $\delta \leq 80$ are based on the kinetic solution of the pressure and temperature-driven flows via the discrete velocity method and for $\delta > 80$ on the corresponding semi-analytical slip solutions. The implemented values of G_P and G_T are grid independent in the physical and velocity spaces up to at least 4 significant digits and are provided as electronic supplementary material. The deduced mass flow rates and pressure differences for the pressure and temperature-driven flows are also considered as accurate up to at least 4 significant digits.

Equation (1) is solved as follows:

- When both end pressures $P(0)$ and $P(2LN)$ are provided, an initial value for the mass flow rate is assumed and Eq. (1) is integrated with the initial condition $P(0)$ along $z \in [0, 2LN]$, using Euler method or a higher-order integration scheme. The computed outlet pressure is compared to the specified $P(2LN)$ and then, the mass flow rate is accordingly corrected depending upon the difference between the computed and specified outlet pressures. This procedure is repeated until $\dot{m}$ and the corresponding $P(z)$ values are converged.
- When mass flow rate $\dot{m}$ with either $P(0)$ or $P(2LN)$ are specified, Eq. (1) is directly integrated along the channel to find the unknown pressure distribution including the pressure at one of the two-channel ends, without requiring an iterative procedure.

In both cases, the values of G_P and G_T are accordingly updated, at each integration step, based on the local cross-section aspect ratio $H(z)/W$ and the local rarefaction parameter $\delta(z)$.

As noted in the introduction the final objective is the fabrication of functional Knudsen pump and diode prototypes based on the multistage designs investigated in the present work. Therefore, following technical discussions with microfabrication experts from Laboratoire d'Architecture et d'Analyse des Systèmes (LAAS), Toulouse, France, some of the design parameters have been specified. The pumps will be manufactured by deposition of dry film photoresist layers on silicon wafers (Courson et al. 2014). Due to the particular fabrication process the channel length, the constant width between the parallel walls (related to the thickness of the dry film layers) and the mean distance (height) between the tapered walls are fixed to $L = 200$ μm, $W = 100$ μm and $\overline{H} = 10$ μm respectively. In addition, due to manufacturing constraints the minimum height $H_{\min} > 1.5$ μm, while the inclination ratio may vary as $1 \leq \alpha \leq 10$. Since $L/\overline{H} = 20$ the assumption of the fully developed flow is justified (Valougeorgis et al. 2017). In addition, in all cases $\overline{H} < W$ and the mean distance $\overline{H}$ remains always the reference length. It is noted that changing the variable height $H(z)$ between the tapered walls has a significant effect on the thermal creep flow, providing different performance characteristics; as a consequence, when $W < \overline{H}$ the width becomes the characteristic length, resulting in negligible pumping and diode effects and this case is not considered here. Furthermore, the temperature at the cold spots is fixed to $T_{\mathrm{C}} = 300$ K, while the temperature at the hot spots is fixed to $T_{\mathrm{H}} = 400$ K. These temperatures and associated lengths are on line with the temperature gradients already applied in accurate measurements of thermally driven flows through glass tubes (Rojas-Cárdenas et al. 2013; Yamaguchi et al. 2014; Rojas-Cárdenas et al. 2011). Finally, the operating pressures may vary in the range $1 - 10^2$ kPa and the carrier gas is a noble monatomic gas. In the present work, the gas is argon (Ar), unless it is otherwise specified. The above data result in rarefied gas flows from the transitional up to the slip regimes with $\delta = 0.1 - 2 \times 10^2$.

In the next section, a detailed computational investigation is performed for the four examined designs in a wide range of the involved not fixed geometric and flow parameters, to develop comprehensive guidelines concerning the expected performance characteristics of the multistage pumps and diodes.

3 Results and discussion

The investigation includes the computed mass flow rate $\dot{m}$ with associated pressure difference $\Delta P = P(2LN) - P(0)$ and pressure distribution $P(z)$, of the four multistage assemblies, in terms of the geometric and operation parameters, taking into account all fabrication, operation and modeling constraints stated above. It is expected that as ΔP is increased, the net mass flow rate $\dot{m}$ is decreased (Tatsios et al. 2017). The two limiting scenarios are as follows: the maximum mass flow rate, $\dot{m}_{\max}$, is obtained when the assembly ends are open and at the same pressure ($\Delta P = 0$), while the maximum pressure difference, $\Delta P_{\max}$, is achieved when the assembly ends are closed ($\dot{m} = 0$). The input parameters include inlet pressure P_{in}, inclination parameter α and number of stages N.

In Sect. 3.1 the characteristics of thermal creep flows through single channels with converging, diverging and constant cross sections, as well as single-stage pumping performances are presented. Then, in Sect. 3.2, the multistage "uni–uni", "con–uni", "div–uni" and "con–div" assemblies are analyzed in terms of a number of stages and associated pump characteristics curves. Finally, in Sect. 3.3, the investigation is focused on the "con–div" assembly to demonstrate its potential as a thermally driven diode for bidirectional pumping, flow blocking and gas separation.

3.1 Single-stage pumping

The characterization of single channels is provided in Sect. 3.1.1, followed by the characterization of single-stage assemblies, consisting of two single channels, in Sect. 3.1.2.

3.1.1 Single-channel characterization

The long rectangular tapered channels considered here, have fixed length $L = 200$ μm, width $W = 100$ μm and mean height $\overline{H} = 10$ μm with inclination parameter $\alpha = [1, 3, 5, 7, 10]$. The corresponding minimum and maximum heights are tabulated in Table 1. The mean height is kept the same to compare the various channels ("con", "div" and "uni") on the same basis (i.e. same reference length), while the cold and hot temperatures are $T_{\mathrm{C}} = 300$ K and $T_{\mathrm{H}} = 400$ K, respectively. For these single rectangular tapered channels, detailed results for the maximum mass flow rate $\dot{m}_{\max}$, corresponding to $\Delta P = 0$, and for the maximum pressure difference $\Delta P_{\max}$, corresponding to $\dot{m} = 0$, are presented in Figs. 2 and 3, respectively, in terms of inlet pressure $P(0) = P_{in} = 1 - 10^2$ kPa. The corresponding inlet values of the gas rarefaction parameter are $\delta = 0.1 - 2 \times 10^2$.

Table 1 Geometry of rectangular tapered channels with $L = 200$ μm, $W = 100$ μm, $\overline{H} = 10$ μm and various inclination parameters α

α	1	3	5	7	10
$H_{\min}$ (μm)	10	5	3.33	2.5	1.82
$H_{\max}$ (μm)	10	15	16.67	17.5	18.2

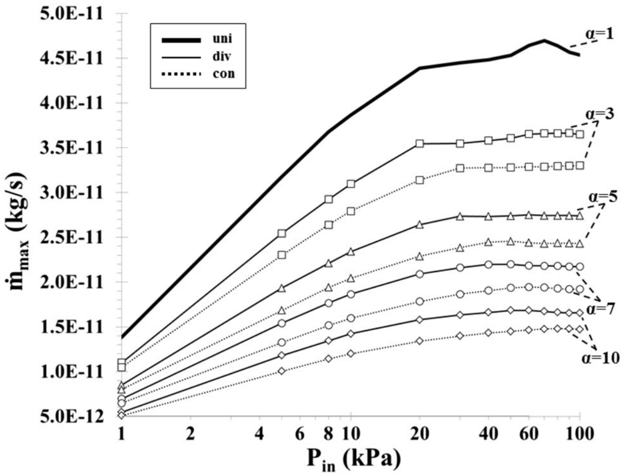

Fig. 2 Maximum mass flow rate $\dot{m}_{\max}$ ($\Delta P = 0$) in terms of inlet pressure P_{in} for thermal creep flow through rectangular channels of converging (con), diverging (div) and uniform (uni) cross sections with inclination parameter $\alpha = [1, 3, 5, 7, 10]$ ($L = 200$ μm, $W = 100$ μm, $\overline{H} = 10$ μm)

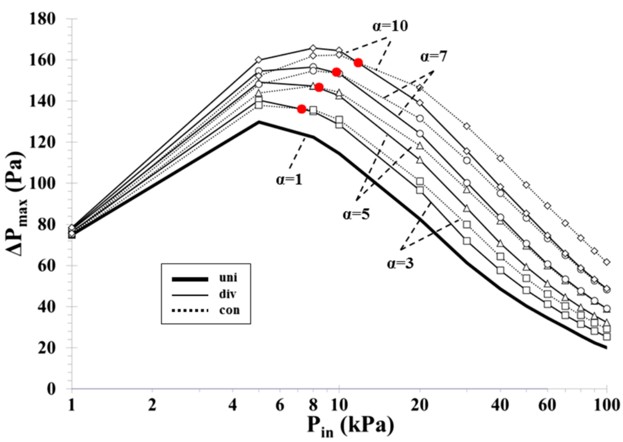

Fig. 3 Maximum pressure difference $\Delta P_{\max}$ ($\dot{m} = 0$) in terms of inlet pressure P_{in} for thermal creep flow through rectangular channels of converging (con), diverging (div) and uniform (uni) cross sections with inclination parameter $\alpha = [1, 3, 5, 7, 10]$ ($L = 200$ μm, $W = 100$ μm, $\overline{H} = 10$ μm); the red dots refer to the blocking inlet pressure P^*_{in}, where $\Delta P_{\max}$ obtained by converging and diverging channels with the same inclination ratio α are equal

In Fig. 2, it is shown that $\dot{m}_{\max}$ is monotonically increased as $P_{\rm in}$ is increased from 1 kPa up to about 50 kPa, corresponding to the transition up to the slip regimes. Then, as the inlet pressure is further increased and the flow is in the hydrodynamic regime, the maximum mass flow rate tends to a constant value. The inclination parameter has clearly a significant effect. More specifically, for the same $P_{\rm in}$ and although the mean height $\overline{H} = 10$ μm is constant, as α is decreased the maximum mass flow rate is increased, with the uniform cross-section channel ($\alpha = 1$) delivering the largest mass flow rates compared to all tapered channels. This is due to the narrowing in the inlet or in the outlet of the diverging and converging channels respectively, as the inclination parameter is increased. Comparing tapered channels with the same inclination parameter α, it is observed that the mass flow rate in the diverging channel is always larger than in the corresponding converging one. This may be contributed to the presence of the deduced pressure-driven flow, which is in the counter-flow direction of the temperature-driven flow. It has been confirmed that in pressure-driven flow the mass flow rate of the converging channel is the larger one (Szalmás et al. 2015; Graur et al. 2016). Therefore, in the present temperature-driven flow setup the overall (net) mass flow rate of the converging channel may be expected to be smaller compared to the corresponding diverging one. The different mass flow rates indicate the presence of a diode effect on the mass flow rate. The computed $\dot{m}_{\max}$ in the whole range of the examined inlet pressure is of the order of 10^{-11} kg/s.

In Fig. 3, it is seen that $\Delta P_{\max}$ has a non-monotonic behavior in terms of $P_{\rm in}$ and more specifically, it initially increases, reaching a peak value $\Delta P^{\rm peak}_{\max}$ at moderate values of $P_{\rm in}$ and then, as $P_{\rm in}$ is further increased it decreases. This non-monotonic behavior, resulting in two regions, for $\Delta P_{\max}$ versus $P_{\rm in}$, one increasing and the other one decreasing, is important and will be implemented, later on, to explain some of the observed technical characteristics of the assemblies. Furthermore, the computed maximum pressure differences $\Delta P_{\max}$ vary from 20 Pa up to 170 Pa. In all cases the peak values of the maximum pressure differences are occurring in the range of $P_{\rm in} = 5 - 10$ kPa, corresponding to gas rarefaction parameters $\delta \approx 4 - 6$, i.e., in the transition regime. This behavior has also been experimentally observed in tubes with uniform circular cross section (Rojas-Cárdenas et al. 2011). The inclination parameter has again a significant effect but now in the opposite way, i.e., as α decreases the maximum pressure difference also decreases, with the uniform cross-section channel ($\alpha = 1$) providing the lowest pressure differences compared to all tapered channels at the same inlet pressures. Clearly, as the inclination ratio is increased, the narrowing of the channel inlet or outlet results in larger pressure differences. In addition, as α is increased, the largest values of the maximum pressure difference, $\Delta P^{\rm peak}_{\max}$, are observed at slightly higher values of $P_{\rm in}$. More importantly, comparing tapered channels with the same inclination parameter α, it is observed that at some specific inlet pressures, defined as blocking inlet pressures P^*_{in}, the maximum pressure differences $\Delta P_{\max}$ obtained by the converging and diverging channels are the same. In Fig. 3, these crossing points are marked by red dots. In the region where $P_{\rm in} < P^*_{\rm in}$, $\Delta P_{\max}$ for the diverging channel is larger than for the corresponding converging one, while in the region where $P_{\rm in} > P^*_{\rm in}$ the situation is reversed. This

Table 2 Blocking inlet pressure P_{in}^{*} in rectangular tapered channels with $L = 200$ µm, $W = 100$ µm, $\overline{H} = 10$ µm and various inclination parameters α ($T_C = 300$ K, $T_H = 400$ K, working gas is Ar)

α	3	5	7	10
P_{in}^{*}(kPa)	7.20	7.92	9.96	12.2

indicates the presence of a diode effect on the pressure difference. For clarity purposes, it is noted that, in general, the blocking inlet pressures P_{in}^{*} are different from the values of P_{in} for which the peak maximum pressure differences ΔP_{max}^{peak} are observed. They both appear, however, in the transition regime. The blocking inlet pressure, P_{in}^{*}, depending on α, varies in the range of $P_{in} = 7 - 15$ kPa and the exact values for the examined inclination parameters are provided in Table 2. Crossing points between the ΔP_{max} curves for converging and diverging channels with different inclination ratios ($\alpha_{con} \neq \alpha_{div}$) are also observed at other inlet pressures. Thus, it is possible by accordingly combining converging and diverging channels to obtain positive, negative or zero pressure differences.

3.1.2 Single-stage characterization

Having a clear view of the flow behavior in single rectangular constant (uniform) and tapered cross-section channels, the flow characteristics of single-stage pumps for the "uni–uni", "con–uni", "div–uni" and "con–div" assemblies are now investigated and results are provided in Figs. 4 and 5. The cold temperatures are kept at $T(0) = T(2L) = T_C = 300$ K and the hot one at $T(L) = T_H = 400$ K. The length and the width of the single-stage pumps are $2L = 400$ µm and $W = 100$ µm, respectively, and the inclination parameter is $\alpha = 7$. Thus, according to Table 1 (see also Fig. 2), the "con–div" assembly consists of two tapered channels with $H_{min} = 2.5$ µm, $H_{max} = 17.5$ µm and $\overline{H} = 10$ µm. The "con–uni" and "div–uni" assemblies consist of one tapered channel with the same dimensions and one uniform cross-section channel with a height of 17.5 µm and the "uni–uni" assembly consists of two uniform cross-section channels with heights of 10 µm and 17.5 µm. Furthermore, results are presented for typical values of $P_{in} = [1, 8, 50]$ kPa, representing low, moderate and high inlet pressures respectively. The moderate inlet pressure of 8 kPa has been chosen since it is within the range of inlet pressures where the peak values ΔP_{max}^{peak} and blocking inlet pressures P_{in}^{*} have been observed.

In Fig. 4 the pressure distribution along the single-stage of the "uni–uni", "con–uni", "div–uni" and "con–div" configurations is plotted for the closed pump ends scenario, where $\Delta P = \Delta P_{max}$ and $\dot{m} = 0$. In all cases the pressure increases in the first half of the pump ($0 \leq z \leq L$), reaching its highest value at $z = L$ and decreases in the second half

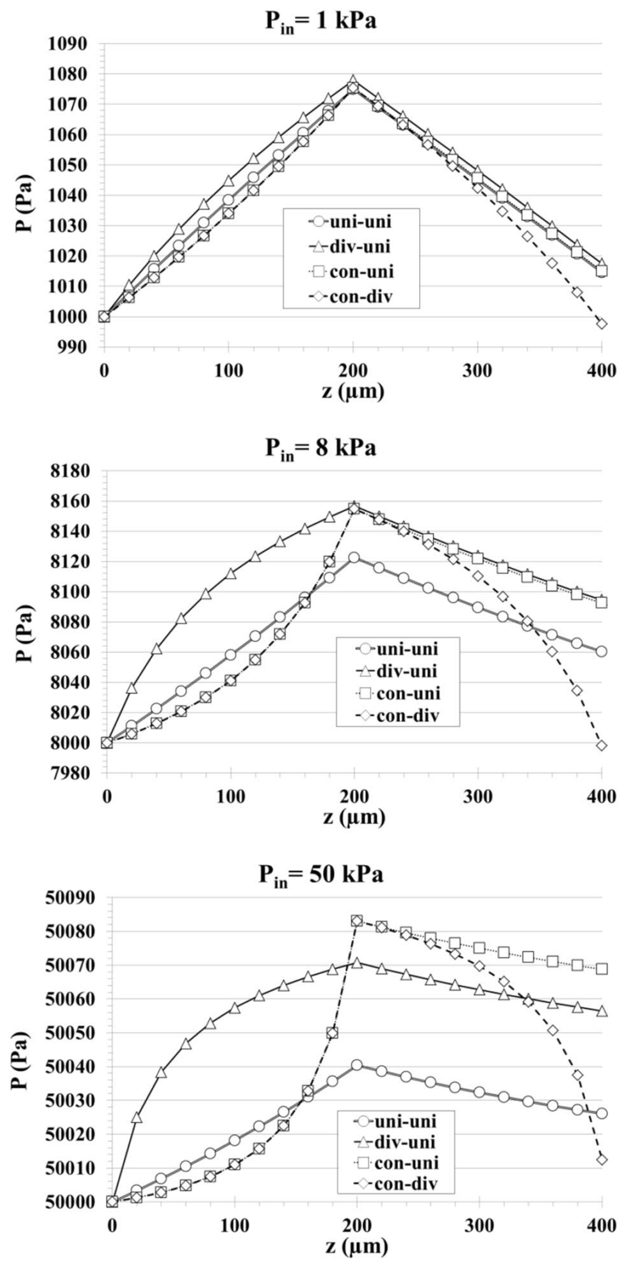

Fig. 4 Pressure distribution along single-stage "uni–uni", "con–uni", "div–uni" and "con–div" assemblies with $\alpha = 7$ for the closed pump ends scenario ($\Delta P = \Delta P_{max}$, $\dot{m} = 0$) at inlet pressure $P_{in} = [1, 8, 50]$ kPa ($L = 200$ µm, $W = 100$ µm, $\overline{H} = 10$ µm)

($L \leq z \leq 2L$). The total pressure difference achieved by the pump is $\Delta P = P(2L) - P(0)$. In the "uni–uni", "con–uni" and "div–uni" assemblies the pressure difference in the first channel is always larger than in the second one for all inlet pressures and $\Delta P > 0$. On the contrary in the "con–div" assembly, depending on the operating pressure P_{in}, ΔP may be positive or negative. More specifically, at $P_{in} = 1$ kPa and 8 kPa the converging channel ($0 \leq z \leq L$) provides a smaller pressure difference than the diverging channel ($L \leq z \leq 2L$)

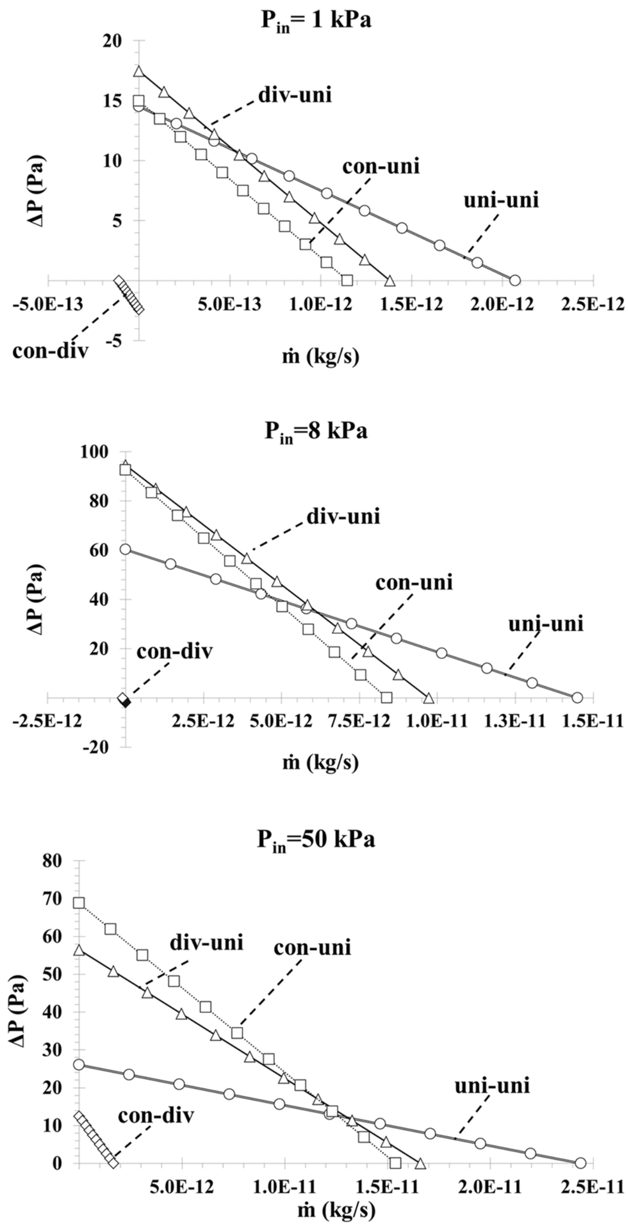

Fig. 5 Characteristic curves of single-stage “uni–uni”, “con–uni”, “div–uni” and “con–div” assemblies with $\alpha = 7$ at inlet pressure $P_{in} = [1, 8, 50]$ kPa ($L = 200$ μm, $W = 100$ μm, $\overline{H} = 10$ μm)

resulting in $\Delta P < 0$, while at $P_{\text{in}} = 50$ kPa, $\Delta P > 0$. It is noted that in the former case $P_{\text{in}} < P^*_{\text{in}}$, while in the latter one $P_{\text{in}} > P^*_{\text{in}}$. It may be useful to note that the exact blocking pressures in single-stage “con–div” assemblies are not exactly the same but very close to the ones in Table 2 for single channels, (e.g. for $\alpha = 7$ in the single-stage assembly $P^*_{in} = 9.93$ kPa, instead of 9.96 kPa in Table 2). This is happening because in the single-stage setup the inlet pressure in the two channels of the assembly is slightly different. These observations demonstrate the possibility to build a device able to reverse the generated pressure difference when P_{in} becomes larger or smaller than P^*_{in}. Concerning the detailed behavior of the pressure distribution along with the single-stage assembly, it depends on the inlet pressure, channel geometry and gas rarefaction parameter. In channels with constant cross sections, the pressure varies almost linearly, while in tapered channels the variation is nonlinear. More specifically, the pressure distribution curves in converging and diverging channels are convex and concave respectively. In general, nonlinearity becomes more evident as the inlet pressure is increased, i.e. as the flow is less rarefied, as well as the pressure difference is increased. This behavior, which is also qualitatively the same in pressure-driven flows through tapered channels, is contributed to the variation of the gas rarefaction due to the variation of the channel height.

In Fig. 5, the characteristic curves presenting the pressure difference ΔP in terms of mass flow rate $\dot{m}$ are shown for the “uni-uni”, “con-uni”, “div-uni” and “con-div” single-stage pumps at $P_{in} = [1, 8, 50]$ kPa. As expected, in all cases, the pressure difference decreases as the mass flow rate increases. The characteristic curves display a linear trend since only one stage is considered and the output pressure is very close to the inlet one, resulting in limited variation of the gas rarefaction parameter δ and the associated kinetic coefficients G_P and G_T. Of course, if several stages are added in series, the behavior may become nonlinear and this is clearly demonstrated in Sect. 3.2. Regarding the performance of each assembly, the characteristic curves of the “uni–uni” one have always the lowest slope, allowing the highest flow rates. Therefore, “uni–uni” assemblies are well adapted for generating high flow rates with limited pressure differences. However, in cases where higher pressure differences are needed with moderate mass flow rates, the “con–uni” and “div–uni” assemblies are more effective. The differences in the characteristic curves of the “con–uni” and “div–uni” assemblies are related to whether the converging or the diverging channel provides higher pressure difference at the specific inlet pressure. In the “con–div” assembly, the diode effect is clearly observed. More specifically, $\Delta P < 0$ when $P_{in} < P^*_{in}$ and $\Delta P > 0$ when $P_{in} > P^*_{in}$, which are exactly the cases for $P_{in} = 1$ kPa and $P_{in} = 50$ kPa respectively. In the former case, the negative values of ΔP and $\dot{m}$ imply that the flow is in the opposite direction compared to all others. At $P_{in} = 8$ kPa the inlet pressure is very close to the blocking inlet pressure $P^*_{in} = 9.93$ kPa and therefore, the characteristic curve is reduced to almost a point at the coordinates’ origin, indicating that both the mass flow rate and the pressure difference are very close to zero. These remarks demonstrate the possibility to build a device, based on the “con–div” configuration, able not only to reverse the pressure difference as noted above but also to reverse the flow when the inlet pressure P_{in} becomes larger or smaller than the blocking inlet pressure P^*_{in}.

In addition to $\alpha = 7$, other values of the inclination parameter have been considered, providing results with the same qualitative behavior and therefore, they are not presented. Based on the investigation of the single-stage assemblies, it may be stated that the "con–uni" and "div–uni" assemblies, providing higher pressure differences and smaller mass flow rates compared to the "uni–uni" assembly, are more suitable in specific pumping applications, where high-pressure drop is required. On the other hand, the "con–div" assembly, providing very small bi-directional net pressure differences and mass flow rates, is suitable in diode applications. These remarks are further investigated in the next section where multistage assemblies are examined.

3.2 Multi-stage pumps and diodes

The performance of multi-stage assemblies is examined in terms of number of stages, type of assembly and operating conditions. The "uni–uni", "con-uni" and "div-uni" assemblies are presented all together and are compared to each other (Figs. 6 and 7). The "con–div" assembly is presented separately (Figs. 8 and 9) for clarity purposes, because its mass flow rates are one order of magnitude smaller than the corresponding ones of the other designs, while the flow may be bi-directional. The geometrical characteristics and the temperature distribution of each stage of the multi-stage assembles are the ones reported in Sect. 3.1. Also, the

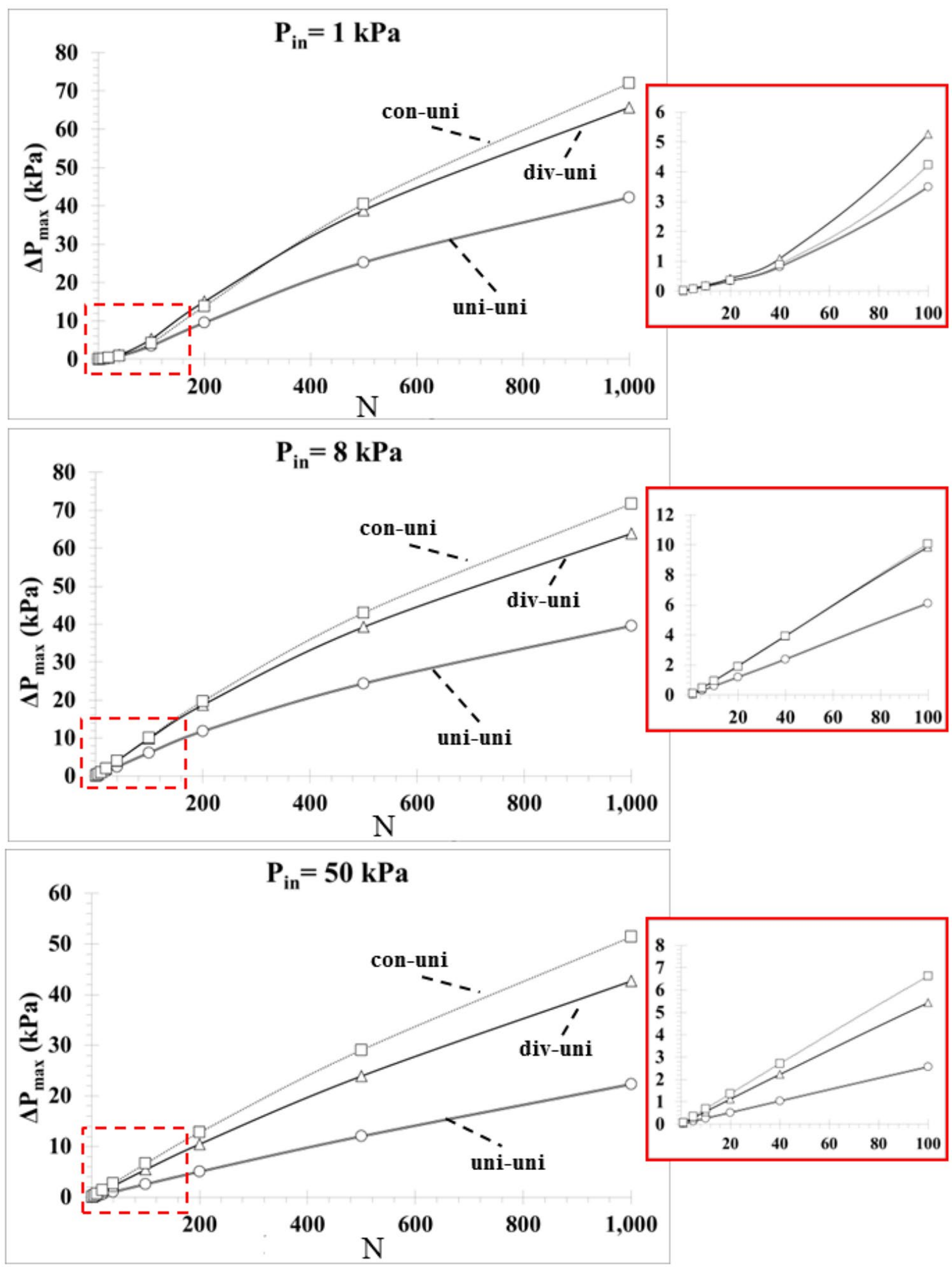

Fig. 6 Maximum pressure difference ΔP_{max} ($\dot{m} = 0$) in terms of number of stages $N = [1 - 1000]$ for "uni–uni", "con–uni" and "div–uni" assemblies with $\alpha = 7$ at inlet pressure $P_{in} = [1, 8, 50]$ kPa ($L = 200$ µm, $W = 100$ µm, $\overline{H} = 10$ µm). The detailed views show the first 100 stages

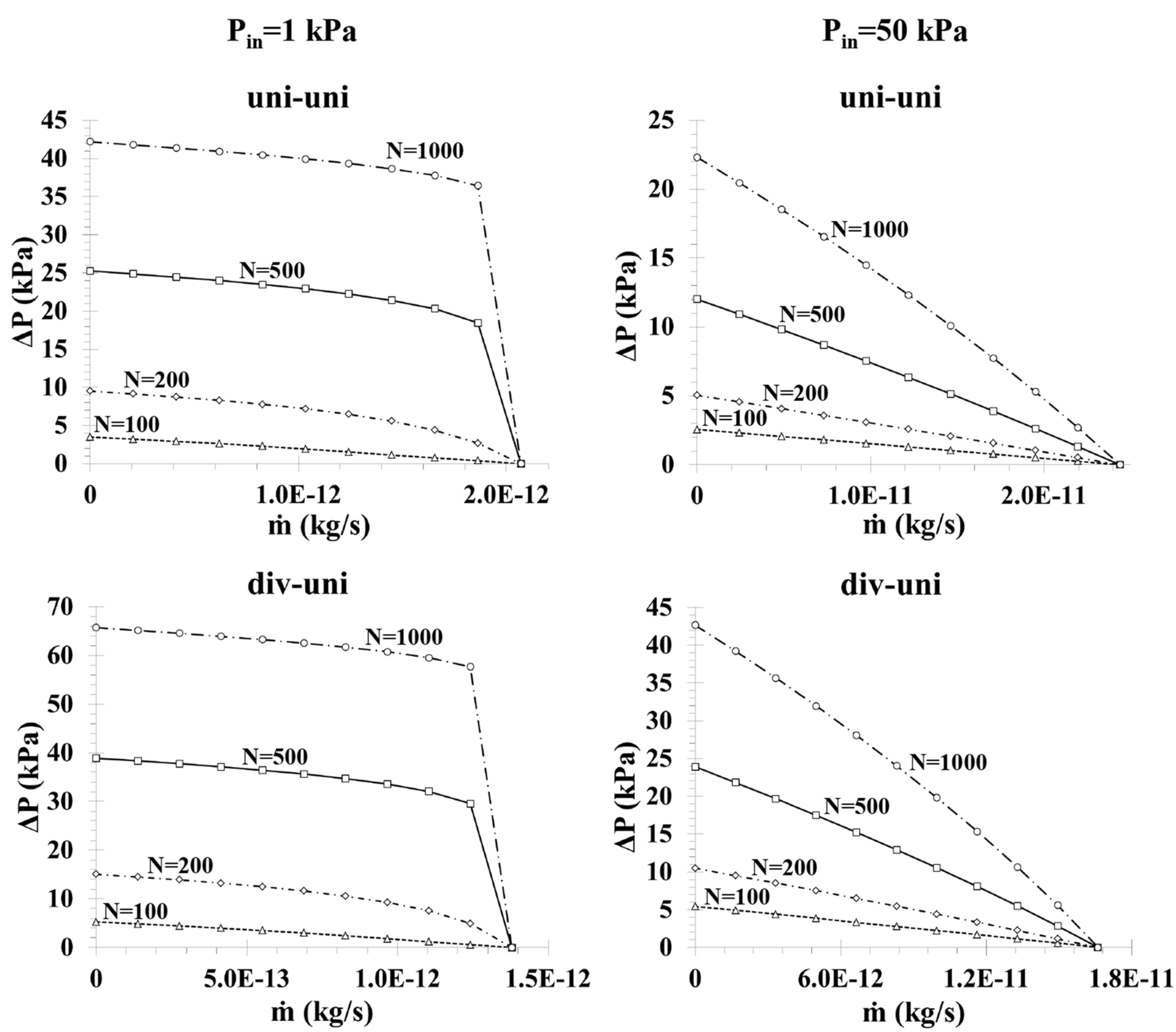

Fig. 7 Characteristic curves of "uni–uni" and "div–uni" multi-stage assemblies with $\alpha = 7$ and $N = [100, 200, 500, 1000]$ at inlet pressure $P_{\text{in}} = [1, 50]$ kPa ($L = 200$ µm, $W = 100$ µm, $\overline{H} = 10$ µm)

inclination parameter is fixed at $\alpha = 7$, while the number of stages N is ranging from one up to a few thousands.

In Fig. 6, the maximum pressure difference $\Delta P_{\max}$ (corresponding to $\dot{m} = 0$) is plotted in terms of number of stages $N = [1 - 1000]$ for the "uni–uni", "con–uni" and "div–uni" assemblies at inlet pressure $P_{in} = [1, 8, 50]$ kPa. As expected, $\Delta P_{\max}$ increases with N. For a small number of stages, $\Delta P_{\max}$ increases rapidly and then it keeps increasing with N, but with a gradually decreasing pace as the number of stages is increased. The rapid increase of $\Delta P_{\max}$ in the first stages is observed more clearly in the detailed views for $N \leq 100$, included in Fig. 6. This behavior has also been reported in (Aoki et al. 1084; López Quesada et al. 2019) and it is due to the varying inlet pressure at each stage, which increases with N. As shown in Fig. 3, as the inlet pressure is increased, the pressure difference increases up to a specific value, where $\Delta P_{\max}^{peak}$ is reached and then it decreases. Therefore, depending on the inlet pressure at each pump stage and on whether this stage operates in the ascending or descending regions of $\Delta P_{\max}$, the resulting maximum pressure difference of the stage may be larger or smaller than of the previous one. As seen in Fig. 6, when the inlet pressure in the first stage is $P_{in} = 1$ kPa and $N < 200$ the pressure difference gained by adding a new stage is larger than of the previous one, while when $N > 200$ it is smaller. This description remains qualitatively the same at $P_{in} = 8$ kPa, where the transition occurs at a much smaller number of stages. When the inlet pressure in the first stage is $P_{in} = 50$ kPa, which is higher than the inlet pressure corresponding to $\Delta P_{\max}^{peak}$ (see Fig. 3), the pressure difference gained by adding a stage is always

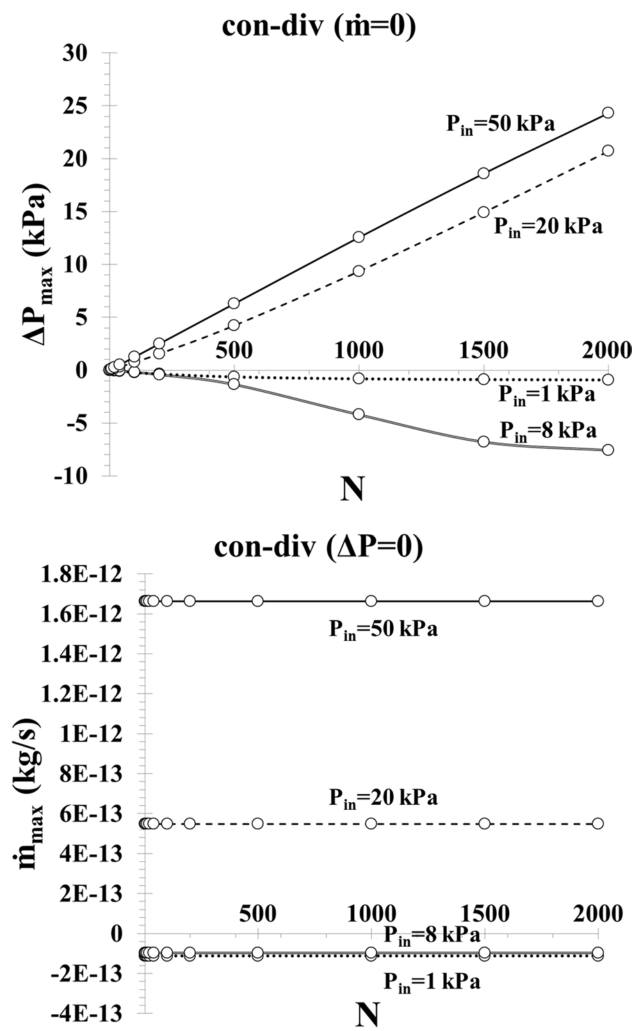

Fig. 8 Maximum pressure difference $\Delta P_{\max}$ ($\dot{m} = 0$) and maximum mass flow rate $\dot{m}_{\max}$ ($\Delta P = 0$) in terms of number of stages $N = [1 - 2000]$ for "con–div" multi-stage assembly with $\alpha = 7$ at inlet pressure $P_{in} = [1, 8, 20, 50]$ kPa ($L = 200$ μm, $W = 100$ μm, $\overline{H} = 10$ μm)

smaller than the previous one. Furthermore, comparing the results between the three configurations, it is observed that the "con–uni" and "div–uni" assemblies have similar performances and always provide larger maximum pressure differences compared to the "uni–uni" case. The obtained maximum pressure difference by the "con–uni" assembly may be larger or smaller compared to the "div–uni" one, depending on whether the inlet operating pressure is above or below P_{in}^{*}. More specifically, the "div–uni" assembly provides slightly higher $\Delta P_{\max}$ at $P_{in} = 1$ kPa and $N < 500$, as well as at $P_{in} = 8$ kPa and $N < 100$, while in all other cases the "con–uni" assembly works slightly better. All these remarks are in agreement with the corresponding single-stage results.

The corresponding maximum mass flow rates $\dot{m}_{\max}$ (associated with $\Delta P = 0$) in terms of N are not presented since they do not depend on the number of stages. This is readily justified by considering that for each assembly, all stages have the same geometry and the same inlet and outlet pressures equal to P_{in}. The maximum mass flow rates are the ones given in Fig. 5 for a single-stage, with $\Delta P = 0$. Comparing the results between the three assemblies, it is found that the maximum mass flow rate of the "uni–uni" assembly is about 1.5 times higher than the corresponding "div–uni" one, which is always slightly larger than the "con–uni" one. In addition, the inlet pressure has a significant effect on the maximum mass flow rate, which is monotonically reduced from the order of 10^{-11} kg/s at $P_{in} = 50$ kPa down to the order of 10^{-12} kg/s at $P_{in} = 1$ kPa.

In Fig. 7, the characteristic curves presenting ΔP in terms of $\dot{m}$ are shown for the "uni–uni" and "div–uni" multistage assemblies, with $N = [100, 200, 500, 1000]$ at inlet pressure $P_{in} = [1, 50]$ kPa. The corresponding results with the "con–uni" assembly are omitted since they are close to the ones of the "div–uni" assembly. As expected, ΔP always decreases as $\dot{m}$ increases. For a specified mass flow rate, the generated pressure difference increases with the number of stages and similarly, for a specified pressure difference, the produced mass flow rate increases with the number of stages. The mean slope of the characteristic curves increases with the number of stages, which is justified by the fact that as N increases, $\Delta P_{\max}$ increases, while $\dot{m}_{\max}$ remains constant. Furthermore, it is seen that the characteristic curves for $N = 100$ at $P_{in} = 1$ kPa, as well as for $N \leq 500$ at $P_{in} = 50$ kPa, are close to linear since in the former case the inlet pressure is small and in the latter one the inlet and output pressures are relatively close to each other. However, as N is increased, the outlet pressures are further increased and the kinetic coefficients G_P and G_T along the pump stages have large variations, resulting in nonlinear characteristic curves. This behavior is much more evident in the low input pressure scenario ($P_{in} = 1$ kPa), where the outlet pressure increases many times more than in the high input pressure scenario ($P_{in} = 50$ kPa). It is interesting to note that at low inlet pressure $P_{in} = 1$ kPa and large number of stages, e.g. $N = [500, 1000]$, the pressure difference starts decreasing very slowly as the mass flow rate increases and then, when $\dot{m}$ approaches its maximum value $\dot{m}_{\max}$, the pressure difference abruptly decreases. This behavior, which is not observed at high inlet pressure $P_{in} = 50$ kPa, is beneficial for assemblies operating at low inlet pressures, for which the flow rate can be significantly increased with a moderate reduction of the pressure difference. Comparing the two assemblies, it may be stated that for the same inlet pressure and number of stages, the "div–uni" assembly delivers higher pressure differences and lower mass flow rates than the corresponding ones of the "uni–uni" assembly. The data for the intermediate inlet pressure $P_{in} = 8$ kPa are not provided since they are in between the reported ones, without exhibiting a specific

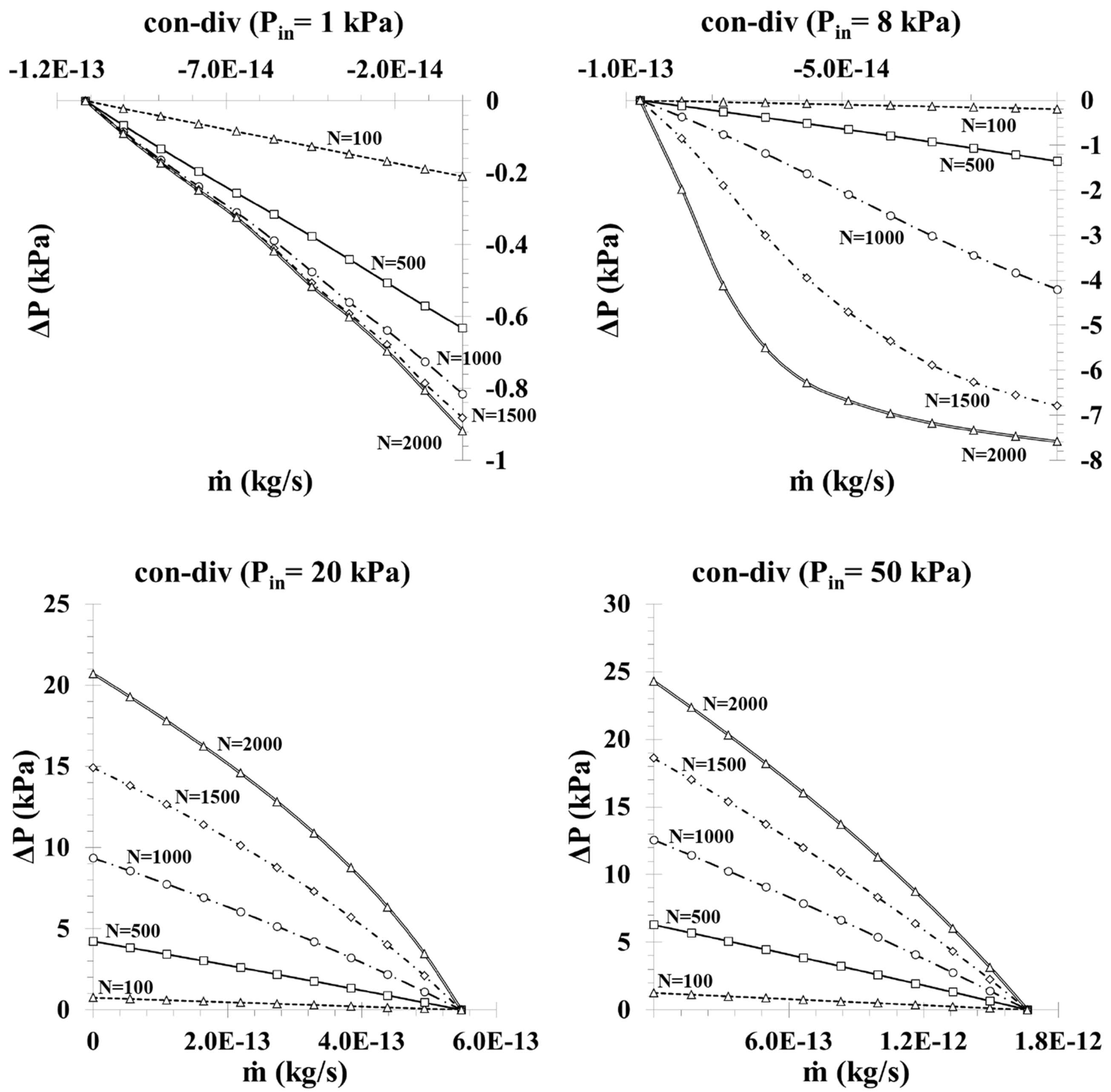

Fig. 9 Characteristic curves of "con–div" multi-stage assembly with $\alpha = 7$ and $N = [100, 500, 1000, 1500, 2000]$ at inlet pressure $P_{in} = [1, 8, 20, 50]$ kPa ($L = 200$ μm, $W = 100$ μm, $\overline{H} = 10$ μm)

behavior. Results for the multi-stage "uni–uni", "con–uni" and "div–uni" assemblies, with $\alpha = 3$, 7 and 10 are also not reported since they are qualitatively similar with the ones presented here for $\alpha = 7$, taking however into consideration that in general, as the inclination parameter increases, the pressure difference increases and the mass flow rate decreases.

The "con–div" assembly is now examined. It is noted that in the "uni–uni", "con–uni" and "div–uni" assemblies the pressure difference and the mass flow rate generated by the first channel of each stage are always larger than the ones in the second channel. Therefore, the net pressure difference is always larger than zero and the mass flow rate in the positive $z-$ direction. On the contrary, in the "con–div" assembly, where the performance characteristics of the converging and diverging channels are very close to each other, depending on whether $P_{in} \lessgtr P^*_{in}$, the net pressure difference and mass flow rate may be either larger or smaller than zero, corresponding to flows in the positive or negative $z-$ direction respectively.

In Fig. 8, the maximum pressure difference $\Delta P_{\max}$ (corresponding to $\dot{m} = 0$) and maximum mass flow rate $\dot{m}_{\max}$ (corresponding to $\Delta P = 0$) are provided in terms of a number of stages $N = [1 - 2000]$ for the "con–div" assembly at inlet pressure $P_{in} = [1, 8, 20, 50]$ kPa. It is seen that for $P_{in} = [20, 50]$ kPa, which are larger than $P^*_{in} = 9.93$ kPa, the flow is in the positive $z-$ direction and the qualitative behavior is similar to the one shown in Fig. 7 for the "uni–uni", "con–uni" and "div–uni" assemblies. On the contrary, for $P_{in} = [1, 8]$ kPa, which are smaller than P^*_{in}, $\Delta P_{\max}$ and $\dot{m}_{\max}$ are negative, indicating that the flow is in the negative $z-$ direction. It is also seen that for $P_{in} = [1, 8]$ kPa, the absolute value of $\Delta P_{\max}$ is increased with the number of stages only until $\left|\Delta P_{\max}\right|$ reaches the inlet pressure P_{in}, since at $\Delta P = -P_{in}$ absolute vacuum is reached and the pressure cannot be further decreased. Concerning the maximum mass flow rate, it is seen that although its absolute value increases as P_{in} increases from 8 to 20 kPa and then to 50 kPa, the reported $\dot{m}_{\max}$ for $P_{in} = 1$ kPa and $P_{in} = 8$ kPa are almost identical. A more detailed investigation by considering various inlet pressures has revealed that in the "con–div" multistage assembly, $\left|\dot{m}_{\max}\right|$ does not increase monotonically with P_{in}. This is due to the fact that the mass flow rates of the converging and diverging channels are very close to each other and the absolute net mass flow rate varies in a nonmonotonic way in terms of inlet pressure.

In Fig. 9, the characteristic curves presenting ΔP in terms of $\dot{m}$ are shown for the "con–div" multi-stage assembly, with $N = [100, 500, 1000, 1500, 2000]$ at inlet pressure $P_{in} = [1, 8, 20, 50]$ kPa. At $P_{in} = [20, 50]$ kPa the inlet pressure is larger than the blocking inlet pressure P^*_{in} and the characteristic curves resemble the performance of the ones displayed in Fig. 7 for the other assemblies, while at $P_{in} = [1, 8]$ kPa the inlet pressure is below P^*_{in} and the flow is reversed, with ΔP and $\dot{m}$ taking negative values. In this latter case, as discussed in Fig. 8, since $\left|\Delta P_{\max}\right|$ cannot be higher than the inlet pressure P_{in}, as N increases, the characteristic curves are converging towards some asymptotic curves. This behavior is evident at $P_{in} = 1$ kPa, where the characteristic curves for $N = [1000, 1500, 2000]$ are very close to each other and less clearly observed at $P_{in} = 8$ kPa, where the corresponding characteristic curves are still far apart. In both cases, the limited characteristic curves will be reached for $N > 2000$. It is pointed out that the absolute values of ΔP and $\dot{m}$ of the "con–div" multi-stage assembly are significantly smaller than the corresponding ones for the other assemblies. Therefore, this configuration is not efficient for pumping purposes. However, by exploiting its diode characteristics (bidirectional pumping and flow blocking), it is quite promising as a microfluidic flow controller or gas mixture separator. These issues are further investigated in the next subsection.

3.3 Parametric study of the blocking inlet pressure in tapered diodes

Having demonstrated the potential of the "con–div" assembly to operate as thermally driven diode at inlet pressures ranging close to the blocking inlet pressure, it is interesting to perform a parametric study of P^*_{in}. It is evident that P^*_{in} depends on the inclination parameter α (see Table 2), while it is expected to depend also on the channel geometry, the temperature difference ΔT driving the flow and the gas species. Furthermore, P^*_{in} is independent of the number of stages N.

Based on the above remarks, single-stage "con–div" assemblies, with various values of the inclination parameter of the diverging channel are considered, taking into account the fabrication constraints. As pointed out in Sect. 3.1.1, different blocking inlet pressures are obtained for converging and diverging channels with different inclination ratios. Therefore, the inclination parameter of the converging channel is kept constant ($\alpha_{con} = 7$), while the inclination parameter of the diverging channel is varied as $\alpha_{div} = [2.5 - 8.5]$. The variation of the blocking inlet pressure P^*_{in} is plotted versus α_{div} and the effect of mean height $\overline{H}$, temperature difference ΔT and working gas species are examined in Figs. 10, 11 and 12, respectively. The assembly length is always $2L = 400$ µm and its width is $W = 100$ µm. The two ends of the single-stage "con–div" assemblies are considered as closed with $\dot{m} = 0$. As shown in Figs. 10, 11, 12, as α_{div} increases, P^*_{in} also increases, covering almost three orders of magnitudes from 0.1 kPa up to 10^2 kPa.

In Fig. 10, the blocking inlet pressure P^*_{in} versus the diverging channel inclination parameter α_{div} is shown for $\overline{H} = [5, 10, 20, 40]$ µm. The mean height $\overline{H}$ is the same for the converging and diverging channels. The temperature difference is $\Delta T = 100$ K and the working gas is argon.

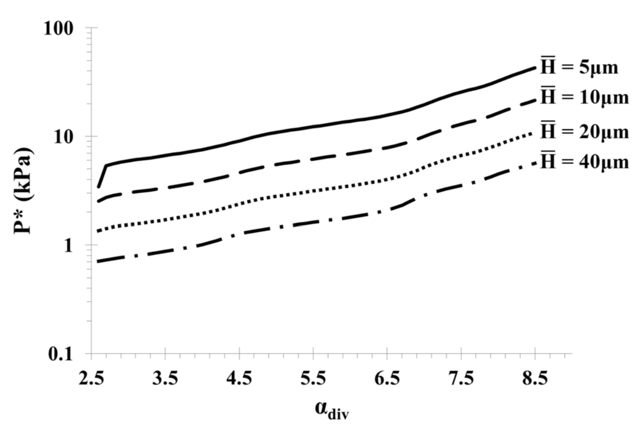

Fig. 10 Inlet blocking pressure P^*_{in} in terms of diverging channel inclination parameter α_{div} for one-stage "con-div" assemblies with $\alpha_{con} = 7$ and $\alpha_{div} = [2.5 - 8.5]$ for $\overline{H} = [5, 10, 20, 40]$ µm ($L = 200$ µm, $W = 100$ µm, $T_C = 300$ K, $\Delta T = 100$ K)

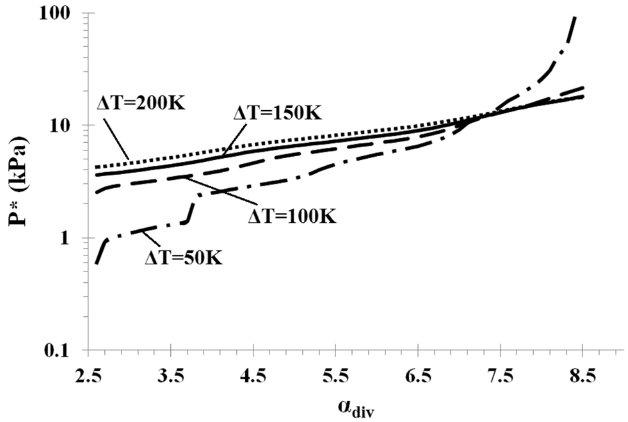

Fig. 11 Inlet blocking pressure P^*_{in} in terms of the diverging channel inclination parameter α_{div} for one-stage "con-div" assemblies with $\alpha_{con} = 7$ and $\alpha_{div} = [2.5 - 8.5]$ for $\Delta T = [50, 100, 150, 200]$ K ($L = 200$ μm, $W = 100$ μm, $\overline{H} = 10$ μm, $T_C = 300$ K)

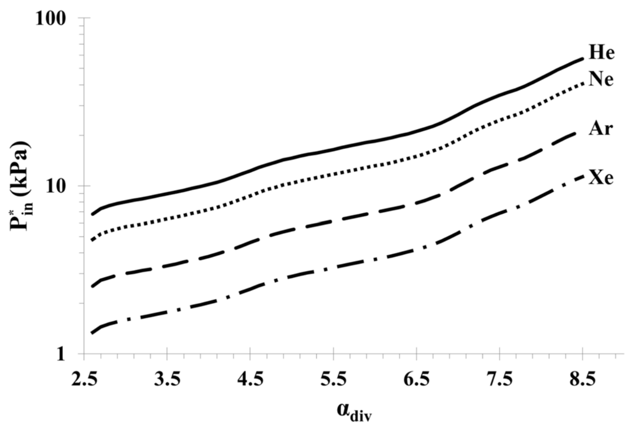

Fig. 12 Inlet blocking pressure P^*_{in} in terms of the diverging channel inclination parameter α_{div} for one-stage "con-div" assemblies with $\alpha_{con} = 7$ and $\alpha_{div} = [2.5 - 8.5]$ for He, Ne, Ar and Xe ($L = 200$ μm, $W = 100$ μm, $\overline{H} = 10$ μm, $T_C = 300$ K, $\Delta T = 100$ K)

It is seen that as $\overline{H}$ decreases, the blocking inlet pressure increases. More specifically, the blocking inlet pressures of the assembly are ranging from $P^*_{in} = [0.7 - 5.6]$ kPa for $\overline{H} = 40$ μm to $P^*_{in} = [1.5 - 42.7]$ kPa for $\overline{H} = 5$ μm. Concerning the other geometric parameters it is noted that the results are independent of L (Tatsios et al. 2017), while the effect of W is found to be negligible, provided that $\overline{H} < W$.

In Fig. 11, P^*_{in} versus α_{div} is shown for $\Delta T = [50, 100, 150, 200]$ K, keeping the cold temperature $T_C = 300$ K. The assembly mean height is $\overline{H} = 10$ μm, while the working gas is argon. As ΔT is increased, the slope of the P^*_{in} versus α_{div} curves is decreased. The largest variation of the blocking inlet pressure is observed at $\Delta T = 50$ K, ranging as $P^*_{in} = [0.3 - 89.2]$ kPa and the smallest one at $\Delta T = 200$ K, ranging as $P^*_{in} = [3.1 - 17.8]$ kPa. It is noted that although the pressure difference varies always linearly with the temperature difference, the associated slope varies with the channel inclination parameter and therefore, the inlet blocking pressure depends on the temperature difference. Furthermore, the curves are crossing each other at about $\alpha_{div} = \alpha_{con}$, where the values of the blocking pressure are approximately the same for different ΔT, due to the fact that the geometrical characteristics of the converging and diverging channels are identical. It is evident that as ΔT increases, the dependency of P^*_{in} on α_{div} reduces and this behavior can be attributed to the relative importance of ΔT and α_{div} on the diverging channel flow. More specifically, for small ΔT the inclination parameter is the dominant quantity affecting the flow, while for large ΔT the temperature difference itself plays the predominant role. At this point, a comment on the jumps occurring for $\Delta T = 50$ K at α_{div} close to 2.7 and 3.8, where P^*_{in} takes small values close to 1 kPa, may be useful. As seen in Fig. 3, the crossing points between the dotted lines for $\alpha_{con} = 7$ and the solid lines for various values of $\alpha_{div} < 7$ move closer to 1 kPa, while the corresponding pressure difference curves are getting very close and almost parallel to each other. As a result, small changes in α_{div} may produce relatively large changes in P^*_{in}. This behavior, observed in Fig. 3, which is for $\Delta T = 100$ K, becomes more evident as ΔT is decreased and therefore the jumps are present for $\Delta T = 50$ K, while there are no jumps for higher temperature differences. It is important to note that unlike $\overline{H}$, which is fixed once the "con–div" assembly is manufactured, the temperature difference ΔT is an operating parameter that can be easily modified by controlling the power input, allowing the easy adjustment of the inlet blocking pressure for a given "con–div" geometry. In general, the variation of P^*_{in} with ΔT is very small when the inclination parameters of the converging and diverging channels are close, but it is getting large when the difference between them is increased. Thus, devices interchanging the pressure difference between two reservoirs in wide or narrow ranges of P^*_{in}, depending upon the target application, may be designed.

In Fig. 12, P^*_{in} versus α_{div} is shown for different working gases, namely helium (He), neon (Ne), argon (Ar) and xenon (Xe), with molecular masses 4.0026, 20.183, 39.948 and 131.3 Da, respectively. The assembly mean height is $\overline{H} = 10$ μm, while the temperature difference is $\Delta T = 100$ K. It is seen that as the gas becomes lighter the inlet blocking pressure is increased. The ranges of the inlet blocking pressure for He, Ne, Ar and Xe are $P^*_{in} = [6.7 - 57.3]$ kPa, $P^*_{in} = [4.8 - 40.6]$ kPa, $P^*_{in} = [2.5 - 21.4]$ kPa and $P^*_{in} = [1.3 - 11.3]$ kPa, respectively. Thus, it is demonstrated that at each specific geometry the blocking inlet pressure between the different monatomic gases is clearly distinguished, implying that the "con–div" assemblies may be designed as part of a microfluidic gas mixture separator.

It is noted that results similar to the ones presented in Figs. 10, 11, 12 have been obtained by keeping the inclination parameter of the diverging channel constant and varying the inclination parameter of the converging channel.

4 Concluding remarks

Thermal transpiration pumping in multistage assemblies consisting of series of long channels with (a) uniform–uniform (“uni–uni”), (b) converging–uniform (“con–uni”), (c) diverging–uniform (“div–uni”) and (d) converging–diverging (“con–div”) rectangular cross sections, have been computationally investigated, parametrized and fully characterized. The analysis is based on the linearized Shakhov kinetic model subject to diffuse boundary conditions. Due to fabrication and operational constraints, the length, width and mean height of each rectangular channel have been fixed as $L = 200$ μm, $W = 100$ μm and $\overline{H} = 10$ μm respectively, while the temperature variation is periodic with period $2L$, with the cold and hot temperatures set at $T_C = 300$ K and $T_H = 400$ K. The inclination parameter and the inlet pressure vary as $1 \leq \alpha \leq 10$ and $P_{in} = \left[1 - 10^2\right]$ kPa respectively. The number of stages N varies from one up to a few thousands. The detailed computational investigation of these four assemblies is performed in terms of α, P_{in} and N to obtain the generated pressure difference ΔP and the corresponding mass flow rate $\dot{m}$, including the maximum pressure difference $\Delta P_{\max}$ reached when the assembly ends are closed ($\dot{m} = 0$) and the maximum mass flow rate $\dot{m}_{\max}$ reached when the assembly ends are open and at the same pressure ($\Delta P = 0$).

In single tapered channels, it has been found that as P_{in} is increased, $\dot{m}_{\max}$ is monotonically increased, while $\Delta P_{\max}$ has a non-monotonic behavior resulting in an increasing region and a decreasing region with a peak value at some moderate values of P_{in} in the transition regime. Furthermore, comparing tapered channels with the same α, it has been found that $\dot{m}_{\max}$ in a diverging channel is always larger than in the corresponding converging one, while $\Delta P_{\max}$ in a diverging channel is larger than in the corresponding converging one when $P_{in} < P^*_{in}$, and smaller when $P_{in} > P^*_{in}$, where P^*_{in} is the blocking inlet pressure for which $\Delta P_{\max}$ obtained by the converging and diverging channels are the same.

In multistage assemblies, the characteristic curves of ΔP versus $\dot{m}$ have been obtained for a different number of stages, showing a strongly nonlinear behavior as N is increased. In the “uni–uni”, “con–uni” and “div–uni” assemblies, since the first channel of each stage performs better than the second one, $\Delta P \geq 0$ and $\dot{m} \geq 0$, which corresponds to the operation of typical pumps. On the contrary in the “con–div” assembly, where the performance characteristics of the converging and diverging channels are very close to each other, the flow may be in the positive or negative z–direction, depending on whether $P_{in} \lesseqgtr P^*_{in}$. In any case, $|\Delta P|$ always decreases as $|\dot{m}|$ increases.

In the “uni–uni”, “con–uni” and “div–uni” assemblies both ΔP and $\dot{m}$ are increased with N and therefore it is advisable to add as many stages as possible to increase, depending on the technological application, either one or both of them. The performances of the “con–uni” and “div–uni” assemblies are very close to each other and provide higher ΔP and smaller $\dot{m}$ than the “uni–uni” assembly. It may be concluded that the “con–uni” and “div–uni” assemblies are more suitable in specific pumping applications targeted to high ΔP and moderate $\dot{m}$, while the “uni–uni” assembly is adapted to more general pumping purposes. Interestingly, all multistage pumps are more stable when operating at small inlet pressures, where the pressure difference remains almost constant in a wide range of the corresponding mass flow rates.

In the “con–div” assembly, the characteristic curves qualitatively resemble the performance of the other three assemblies when $P_{in} > P^*_{in}$, while the flow is reversed, with ΔP and $\dot{m}$ taking negative values when $P_{in} < P^*_{in}$. In addition, the absolute values of ΔP and $\dot{m}$ of the “con–div” multi-stage assembly have been found to be significantly smaller than the corresponding ones of the other assemblies. Therefore, this configuration is not effective for pumping purposes and instead, it may be implemented as thermally driven microfluidic diode. To investigate its potential as a diode device, a detailed parametrization study has been performed in single-stage “con–div” assemblies for analyzing the blocking inlet pressure by keeping α_{con} fixed and varying α_{div}, as well as $\overline{H}$, ΔT and the working gas. It has been found that P^*_{in} is very sensitive to all these parameters. By accordingly specifying α_{div}, $\overline{H}$ and ΔT, the blocking inlet pressure may be easily adjusted and various diodes, depending upon the target application, may be designed. The investigation with regard to different monatomic gases has revealed that as the gas becomes lighter, P^*_{in} is increased. Thus, “con–div” assemblies may be ideally applied to separate the species in gas mixtures.

In the near future, tapered-channel prototypes will be experimentally tested to validate the present computational results. Additional modeling and computational work, considering multicomponent gas mixture flow through the “con–div” assembly, is also planned.

Acknowledgements This work has received funding from the European Union’s Framework Programme for Research and Innovation Horizon 2020 (2014–2020) under the Marie Skłodowska-Curie Grant Agreement No. 643095. This work was partly supported by the French Renatech network: The technical information and constraints received from Laboratoire d’Analyse et d’Architecture des Systèmes in Toulouse, France, regarding the manufacturing process to be implemented in the short future are highly acknowledged.

References

Alexeenko AA, Gimelshein SF, Muntz EP, Ketsdever AD (2006) Kinetic modeling of temperature driven flows in short microchannels. Int J Therm Sci 45:1045–1051

An S, Gupta NK, Gianchandani YB (2014) A Si-Micromachined 162-stage two-part knudsen pump for on-chip vacuum. J Microelectromechan Syst 23:406–416

Aoki K, Degond P, Takata S, Yoshida H (2007) Diffusion models for Knudsen compressors. Phys Fluids 19:117103

Aoki K, Mieussens L, Takata S, Degond P, Nishioka M, Takata S (2007) Numerical simulation of a knudsen pump using the effect of curvature of the channel

Aoki K, Takata S, Kugimoto K, Abe T (2008) Diffusion approximation for the knudsen compressor composed of circular tubes In Proceedings of the AIP Conference Proceedings AIP Publishing 1084, pp. 953–958

Aoki K, Degond P, Mieussens L, Takata S, Yoshida H (2008) A Diffusion model for rarefied flows in curved channels. Multiscale Model Simul 6:1281–1316

Bond DM, Wheatley V, Goldsworthy M (2014) Numerical investigation of curved channel Knudsen pump performance. Int J Heat Mass Transf 76:1–15

Bond DM, Wheatley V, Goldsworthy M (2016) Numerical investigation into the performance of alternative Knudsen pump designs. Int J Heat Mass Transf 93:1038–1058

Cheng Q, Qin Y, Gianchandani YB (2017) A bidirectional Knudsen pump with superior thermal management for micro-gas chromatography applications. In Proceedings of the 2017 IEEE 30th International Conference on Micro Electro Mechanical Systems (MEMS); IEEE pp. 167–170.

Chen J, Stefanov SK, Baldas L, Colin S (2016) Analysis of flow induced by temperature fields in ratchet-like microchannels by direct simulation monte carlo. Int J Heat Mass Transf 99:672–680

Chernyak VG, Kalinin VV, Suetin PE (1979) Theory of nonisothermal gas motion in a plane channel. J Eng Phys 36:696–700

Colin S (2014) Single-phase gas flow in microchannels. In *Heat Transfer and Fluid Flow in Minichannels and Microchannels*; Elsevier, pp. 11–102

Courson R, Cargou S, Conedera V, Fouet M, Blatche MC, Serpentini CL, Gue AM (2014) Low-cost multilevel microchannel lab on chip: DF-1000 series dry film photoresist as a promising enabler. RSC Adv 4:54847–54853

Graur I, Ho MT (2014) Rarefied gas flow through a long rectangular channel of variable cross section. Vacuum 101:328–332

Graur I, Sharipov F (2009) Non-isothermal flow of rarefied gas through a long pipe with elliptic cross section. Microfluid Nanofluidics 6:267–275

Graur I, Méolans JG, Perrier P, Thöming J, Veltzke T (2016) A physical explanation of the gas flow diode effect. Microfluid Nanofluidics 20:145

Gupta NK, Gianchandani YB (2011) Porous ceramics for multistage Knudsen micropumps-modeling approach and experimental evaluation. J Micromech Microeng 21:095029

Gupta NK, An S, Gianchandani YB (2012) A Si-micromachined 48-stage Knudsen pump for on-chip vacuum. J Micromechan Microeng 22:105026

Kim SK, Chang H, Zellers ET (2011) Microfabricated gas chromatograph for the selective determination of trichloroethylene vapor at sub-parts-per-billion concentrations in complex mixtures. Anal Chem 83:7198–7206

Knudsen M (1909) Eine Revision der Gleichgewichtsbedingung der Gase. Thermische Molekularströmung Ann Phys 336:205–229

Knudsen M (1910) Thermischer Molekulardruck der Gase in Röhren. Ann Phys 338:1435–1448

Kugimoto K, Hirota Y, Kizaki Y (2016) Motionless heat pump - A new application of thermal transpiration. In Proceedings of the AIP Conference Proceedings; American Institute of Physics Inc., Vol. 1786, p. 080004

Kugimoto K, Hirota Y, Yamauchi T, Yamaguchi H, Niimi T (2018) A novel heat pump system using a multi-stage Knudsen compressor. Int J Heat Mass Transf 127:84–91

Leontidis V, Chen J, Baldas L, Colin S (2014) Numerical design of a Knudsen pump with curved channels operating in the slip flow regime. Heat Mass Transf 50:1065–1080

Liu K, Zhang W, Chen W, Li K, Dai F, Cui F, Wu X, Ma G, Xiao Q (2009) The development of micro-gyroscope technology. J Micromechan Microeng 19:113001

López Quesada G, Tatsios G, Valougeorgis D, Rojas-Cárdenas M, Baldas L, Barrot C, Colin S (2019) Design Guidelines for Thermally Driven Micropumps Of Different Architectures Based On Target applications via kinetic modeling and simulations. Micromachines 10:249

Maxwell JC (1878) On stresses in rarefied gases arising from inequalities of temperature. Proc R Soc London 27:304–308

McNamara S, Gianchandani YB (2005) On-chip vacuum generated by a micromachined Knudsen pump. J Microelectromech Syst 14:741–746

Nakaye S, Sugimoto H (2016) Demonstration of a gas separator composed of Knudsen pumps. Vacuum 125:154–164

Nakaye S, Sugimoto H, Gupta NK, Gianchandani YB (2015) Thermally enhanced membrane gas separation. Eur J Mech B/Fluids 49:36–49

Naris S, Valougeorgis D, Kalempa D, Sharipov F (2005) Flow of gaseous mixtures through rectangular microchannels driven by pressure, temperature, and concentration gradients. Phys Fluids 17:100607

Naris S, Tantos C, Valougeorgis D (2014) Kinetic modeling of a tapered Holweck pump. Vacuum 109:341–348

Ohwada T, Sone Y, Aoki K (1989) Numerical analysis of the Poiseuille and thermal transpiration flows between two parallel plates on the basis of the Boltzmann equation for hard sphere molecules. Phys Fluids A Fluid Dyn 1:2042–2049

Pantazis S, Naris S, Tantos C, Valougeorgis D, André J, Millet F, Perin JP (2013) Nonlinear vacuum gas flow through a short tube due to pressure and temperature gradients. Fusion Eng Des 88:2384–2387

Qin Y, Gianchandani YB (2014) iGC1: An integrated fluidic system for gas chromatography including knudsen pump, preconcentrator, column, and detector microfabricated by a three-mask process. J Microelectromechanical Syst 23:980–990

Qin Y, An S, Gianchandani YB (2015) Arrayed architectures for multi-stage Si-micromachined high-flow Knudsen pumps. J Micromechan Microeng 25:115026

Qin Y, Gianchandani YB (2016) A fully electronic microfabricated gas chromatograph with complementary capacitive detectors for indoor pollutants. Microsystems Nanoeng 2:15049

Reynolds O (1879) XVIII. On certain dimensional properties of matter in the gaseous state. Philos Trans R Soc London Ser A 170:727–845

Ritos K, Lihnaropoulos Y, Naris S, Valougeorgis D (2011) Pressure- and temperature-driven flow through triangular and trapezoidal microchannels. Heat Transf Eng 32:1101–1107

Rojas-Cárdenas M, Graur I, Perrier P, Meolans JG (2011) Thermal transpiration flow: A circular cross-section microtube submitted to a temperature gradient. Phys Fluids 23:031702

Rojas-Cárdenas M, Graur I, Perrier P, Méolans JG (2013) Time-dependent experimental analysis of a thermal transpiration rarefied gas flow. Phys Fluids 25:072001

Rovenskaya OI (2020) Numerical investigation of thermally generated gas flow between saw-tooth like surfaces. Int J Heat Mass Transf 147:118979

Sharipov F (1996) Rarefied gas flow through a long tube at any temperature ratio. J Vac Sci Technol A Vacuum Surfaces Film 14:2627–2635

Sharipov F (1999) Non-isothermal gas flow through rectangular microchannels. J Micromechan Microeng 9:394–401

Sharipov F, Bertoldo G (2005) Rarefied gas flow through a long tube of variable radius. J Vac Sci Technol A Vacuum Surfaces Film. 23:531–533

Sharipov F, Seleznev V (1998) Data on internal rarefied gas flows. J Phys Chem Ref Data 27:657

Sheng Q, Tang G-H, Gu X-J, Emerson DR, Zhang Y-H (2014) Simulation of thermal transpiration flow using a high-order moment method. Int J Mod Phys C 25:1450061

Sone Y (1966) Thermal creep in rarefied gas. J Phys Soc Japan 21:1836–1837

Sone Y (2000) Flows induced by temperature fields in a rarefied gas and their ghost effect on the behavior of a gas in the continuum limit. Annu Rev Fluid Mech 32:779–811

Sone Y (2007) Molecular gas dynamics: theory, techniques, and applications. Springer Science & Business Media, Berlin

Sone Y, Waniguchi Y, Aoki K (1996) One-way flow of a rarefied gas induced in a channel with a periodic temperature distribution. Phys Fluids 8:2227–2235

Szalmás L, Veltzke T, Thöming J (2015) Analysis of the diodic effect of flows of rarefied gases in tapered rectangular channels. Vacuum 120:147–154

Tatsios G, Lopez Quesada G, Rojas-Cardenas M, Baldas L, Colin S, Valougeorgis D (2017) Computational investigation and parametrization of the pumping effect in temperature-driven flows through long tapered channels. Microfluid Nanofluidics 21:99

Valougeorgis D, Vasileiadis N, Titarev V (2017) Validity range of linear kinetic modeling in rarefied pressure driven single gas flows through circular capillaries. Eur J Mech B/Fluids 64:2–7

van Beek JTM, Puers R (2012) A review of MEMS oscillators for frequency reference and timing applications. J Micromechan Microeng 22:013001

Van Toan N, Inomata N, Trung NH, Ono T (2018) Knudsen pump produced via silicon deep RIE, thermal oxidation, and anodic bonding processes for on-chip vacuum pumping. J Micromechan Microeng 28:055001

Vargo SE (2001) Initial results from the first MEMS fabricated thermal transpiration-driven vacuum pump. In Proceedings of the AIP Conference Proceedings; AIP Vol. 585, pp. 502–509

Yamaguchi H, Rojas-Cárdenas M, Perrier P, Graur I, Niimi T (2014) Thermal transpiration flow through a single rectangular channel. J Fluid Mech 744:169–182

Zeng P, Wang K, Ahn J, Ronney PD (2013) Thermal transpiration based pumping and power generation devices. J Therm Sci Technol 8:370–379